

Accepted Manuscript

Light scattering from volcanic-sand particles in deposited and aerosol form

Zubko Nataliya, Muñoz Olga, Zubko Evgenij, Gritsevich Maria, Escobar-Cerezo Jesús, Berg Matthew J, Peltoniemi Jouni



PII: S1352-2310(19)30442-X

DOI: <https://doi.org/10.1016/j.atmosenv.2019.06.051>

Reference: AEA 16813

To appear in: *Atmospheric Environment*

Received Date: 30 January 2019

Revised Date: 31 May 2019

Accepted Date: 24 June 2019

Please cite this article as: Nataliya, Z., Olga, Muñ., Evgenij, Z., Maria, G., Jesús, E.-C., Matthew J, B., Jouni, P., Light scattering from volcanic-sand particles in deposited and aerosol form, *Atmospheric Environment* (2019), doi: <https://doi.org/10.1016/j.atmosenv.2019.06.051>.

This is a PDF file of an unedited manuscript that has been accepted for publication. As a service to our customers we are providing this early version of the manuscript. The manuscript will undergo copyediting, typesetting, and review of the resulting proof before it is published in its final form. Please note that during the production process errors may be discovered which could affect the content, and all legal disclaimers that apply to the journal pertain.

Light scattering from volcanic-sand particles in deposited and aerosol form

Zubko^a, Nataliya; Muñoz^b, Olga; Zubko^c, Evgenij; Gritsevich^{d, e}, Maria; Escobar-Cerezo^d, Jesús ; Berg,
Matthew^f J.; Peltoniemi^a, Jouni

^aFinnish Geospatial Research Institute, Geodeetinrinne 2, 02430 Masala, Finland

^bInstituto de Astrofísica de Andalucía, CSIC Glorieta de la Astronomía s/n, 18008, Granada, Spain

^cSchool of Natural Sciences, Far Eastern Federal University, 8 Sukhanova street, Vladivostok 690950, Russia

^dUniversity of Helsinki, Department of Physics, Gustaf Hällströmin katu 2, 00014 Helsinki, Finland,

^eInstitute of Physics and Technology, Ural Federal University, Mira street 19, 620002 Ekaterinburg, Russia

^fKansas State University, Department of Physics, 1228 North 17th Street, Manhattan, KS 66506-2601, USA

Corresponding author: Nataliya Zubko,

e-mail: nataliya.zubko@nls.fi

Abstract

The light-scattering properties of volcanic sand collected in Iceland are studied here to characterize the sand particles and develop a reference for future remote-sensing observations. While such sand is common in Iceland, the smaller-size fraction can be readily transported by winds and found in the atmosphere at distant locations. The sand appears dark when deposited on a surface due to the high optical absorption of the material. Therefore, atmospheric regions containing such particles during a dust storm may absorb sunlight considerably, causing redistribution of solar energy. Here, we measure the angular scattered-light intensity and degree of linear polarization from the sand. This is done with two experimental apparatuses, the Cosmic Dust Laboratory (CoDuLab) at the Instituto de Astrofísica de Andalucía (IAA) and the goniospectropolarimeter (FIGIFIGO) at the Finnish Geospatial Research Institute (FGI). Two scattering-scenarios of practical interest for remote-sensing applications are

32 considered: (1) single sand-particles suspended in aerosol as an optically thin cloud, and (2) the same
33 particles deposited on a substrate. We also model the measurements with the discrete dipole
34 approximation to estimate the complex-valued refractive index m , where we find that $m \approx 1.6 + 0.01i$ at
35 $\lambda = 647$ nm. Lastly, we present a comparative analysis of the polarimetric response of the sand
36 particles with that reported in the literature for carbon-soot, another highly absorbing atmospheric
37 contaminant.

38
39 **Key words:** volcanic sand; remote sensing; polarimetry; radiometry; photometry; particulate surface;
40 aerosols; light scattering; discrete dipole approximation; refractive index; soot

41

42 1. Introduction

43 One of the largest uncertainties with regard to the interaction of solar radiation between the atmosphere
44 and the Earth-surface, i.e., the Earth's radiative energy budget, is associated with aerosols including
45 dust (Boucher *et al.*, 2013). This work studies Icelandic volcanic sand, a significant source of dust in
46 Northern Europe that is close to arctic glacier (Prospero *et al.*, 2012). In particular, our study reveals a
47 degree of similarity between the optical properties of Icelandic volcanic sand and black carbon
48 particles; specifically, both particle types strongly absorb solar radiation thus heating the atmosphere
49 and reducing the amount of solar energy received at the Earth surface. The majority of black carbon in
50 the atmosphere has anthropogenic origin, while the volcanic sand discussed here is natural in origin.
51 Given its history of volcanic activity, Iceland has experienced an extended period of absorbing-aerosol
52 effects as evidenced by the abundance of volcanic sand, which has led to climatic influences both
53 locally and regionally across the northern latitudes.

54 Volcanic sand is one of the main dust-sources in Iceland due to the abundance of rock of volcanic
55 origin. The weather conditions are favorable for active sand-formation via the erosion of solidified lava
56 flows, and thus, about 20% of Iceland is covered with volcanic sand (Arnalds, 2015). Sandy deserts
57 cover large portions of the south coast and glacial margins of the active volcanic zone from the
58 Mýrdalsjökull glacier to areas northeast of the Vatnajökull glacier (Fig. 1). The desert area near the
59 Mýrdalsjökull glacier can be seen in the enlarged MODIS satellite image along with a visible portion of
60 the contaminated glacier. For a more detailed map of the sand dessert distribution, see Arnalds, 2015
61 (chapter 11).

62 Volcanic sand in Iceland consist mostly of basaltic glass (Arnalds, 2015). Such basaltic
63 volcanic materials can be found in other volcanically active areas such as Hawaii and other states of the
64 USA and in New Zealand (Edgett & Lancaster, 1993), however the composition, particle size
65 distribution, and microphysical properties vary with the place of origin and sand formation factors. It is
66 also worth noting that Iceland has one of the largest volcanoclastic sand-fields (Arnalds *et al.*, 2001).

67 Frequent dust-storms lift small volcanic-sand particles off the surface and transport them over
68 great distances. For instance, they can be deposited in high latitude regions like Svalbard and
69 Greenland (Groot Zwaafink, 2017). Unlike desert sand, which is typically a quartz-mineral (e.g.,
70 Volten *et al.*, 2001; Nousiainen *et al.*, 2009), the composition of volcanic sand is less well known.
71 Nevertheless, what is known about the composition of suspended volcanic sand suggests a significant
72 impact on the atmosphere, specifically across the Northern latitudes (Dagsson-Waldhauserova *et al.*,
73 2016) in addition to its contribution to accelerating glacier melt (Wittmann, 2017).

74 The transport of volcanic sand by wind contaminates both the atmosphere and ground-surface along
75 its transport path, where suspended particles efficiently absorb solar radiation leading to simultaneous
76 heating of the atmosphere and surface. Because the suspended particles eventually settle-out, for

77 instance, on a pure ice and/or snow surface, the surface albedo is altered leading to enhanced heating
78 and an increase in the surface's density (Meinander *et al.*, 2014; Peltoniemi *et al.*, 2015). This in turn
79 triggers melting or evaporation of ice and snow surfaces (Qian, 2009).

80 Contamination of the atmosphere or icy/snow terrestrial surfaces by volcanic sand can be detected
81 with remote-sensing techniques through ground-based and satellite observations (e.g. AERONET,
82 Holben *et al.*, 1998, Sinyuk, *et al.*, 2007, GOME-2: Munro *et al.* 2016, CALIOP/CALIPSO: Winker *et*
83 *al.*, 2009). The reflectance and polarization of sunlight scattered by atmospheric aerosols contain
84 important information about the microphysical properties of the particles. Indeed, polarimetry is a
85 powerful and promising tool for the retrieval and characterization of these microphysical properties.
86 Presently, several space instruments have polarization sensors and provide Earth observational data (e.g.
87 Herman, 2005, Munro *et al.* 2016). Moreover, a number of new space missions are planned, which will
88 perform airborne polarimetry (Dubovik *et al.*, 2019). Interpretation of such measurements, however,
89 remains difficult primarily because the measurements are simultaneously affected by the particles'
90 shape, size distribution, and chemical composition. Comparison of satellite data with ground-based
91 measurements may show significant differences. An example is Tao *et al.*, 2017, who demonstrate an
92 evaluation of the MODIS Deep Blue aerosol algorithm in the desert region of East Asia and compare to
93 retrievals with ground-based observations obtained with China Aerosol Remote Sensing Network.
94 They find that the MODIS-based retrievals of aerosol optical depth can be significantly underestimated.
95 Besides the aerosol optical depth characteristics, aerosol-type classification is another challenge (Kahn
96 & Gaitley, 2015). For instance, a set of dust mixtures is used to define the aerosol type in Multiangle
97 Imaging Spectroradiometer (MISR) retrievals algorithms. Thus, knowledge of the optical properties of
98 various dust types is critical for the success of such retrievals. Laboratory studies of the light scattering

99 properties of dust particles could meaningfully improve the algorithm inputs and interpretation of *in*
100 *situ* measurements.

101 In this work, we investigate the reflectance and degree of linear polarization of sunlight scattered by
102 volcanic-sand particles suspended in air and the same particles deposited on a surface. As such, our
103 experiment reproduces both of measurement scenarios relevant for remote-sensing observations of
104 volcanic sand, i.e., in the atmosphere or deposited on an ice/snow surface. Previous related
105 measurements mainly focus on either single-particles or deposited-particles (Muñoz et al. 2004; 2015;
106 Hadamcik, 2002; Sun 2014; Peltoniemi *et al.*, 2009, Wilkman *et al.*, 2016). There are only few
107 examples where both light-scattering scenarios are simultaneously studied (e.g., Shkuratov *et al.*, 2004,
108 2006; Francis *et al.*, 2011) and Icelandic volcanic sand is not encompassed in that work. The
109 measurements in our work are conducted at two experimental facilities: the
110 goniospectropolarimeter (FIGIFIGO) located at the Finnish Geospatial Research Institute (FGI)
111 and Cosmic Dust Laboratory (CoDuLab) at the Instituto de Astrofísica de Andalucía (IAA). The
112 FIGIFIGO facility (Fig. 2) is designed to measure the light-scattering response from a particle-coated
113 surface (Peltoniemi et al., 2014), whereas the CoDuLab facility (Fig. 3) is used to measure the full
114 scattering-matrix of particles suspended in air (Muñoz et al., 2012). We also complement our study
115 with mass spectrometry to infer the elemental composition of the volcanic sand samples used.

116 Light scattering properties of surface-deposited volcanic sand have, in part, been studied before. In
117 Peltoniemi *et al.* (2015), the sand is used as a highly absorbing contaminant for a snow surface, where
118 that study focus on how the contamination affects the reflection and polarization properties of the snow.
119 In work by Zubko *et al.* (2016), the optical properties of high-contrast two-component mixtures
120 involving volcanic sand are studied, where the sand serves as a dark component among two types of
121 bright components, salt (NaCl) and ferric sulfate ($\text{Fe}_2(\text{SO}_4)_3$). Note, however, that the light-scattering

122 behavior of volcanic sand is investigated in these studies only when the particles are deposited on a
123 substrate (particulate surface). The single-particle regime of light scattering is not yet investigated.

124

125 **2. Sample description**

126 Volcanic-sand particles mainly consist of poorly crystallized glasses of basaltic to andesitic origin. The
127 samples we consider are a mixture of glaciofluvial volcanic ash originating from beneath the
128 Mýrdalsjökull glacier mixed with ash from the Eyjafjallajökull and Grímsvötn eruptions of 2010 and
129 2011, respectively. We choose this sample because it is representative of materials that are typical of
130 aerosol-dust sources in Southern Iceland and the particles deposited on glaciers or snow in that area
131 (Arnalds *et al.*, 2013, Arnalds *et al.*, 2016). Specifically, our samples were collected from the
132 Mýrdalssandur area in Iceland. The large black-colored area in Fig. 1 corresponds to the field of
133 volcanic sand and the upper layer of this sand (about 10 cm thickness) was collected with a shovel.
134 Wind erosion in the area contributes to the redistribution of loose surface material, and according to
135 Arnalds *et al.* 2016, the rates of surface transport of aeolian materials is between 500 and 3,000 kg m⁻¹
136 year⁻¹. This means that about 0.5–3 tons are blown over a 1 m wide transect each year. The relevant
137 volcanic sand formation and erosion processes in Iceland are outlined in more detail, in e.g., (Baratoux
138 *et al.* 2011, Arnalds *et al.* 2013).

139 Our sand samples generally divide into the following categories:

- 140 1) Natural volcanic sand without processing (except for drying);
- 141 2) Sieved volcanic sand where the size of the particles is less than 250 μm , including:
 - 142 a) Dry sand;
 - 143 b) Wet sand, where moisture is provided by an atomizer;
- 144 3) Milled volcanic sand where the particles are ground to produce a fine-grained powder.

145 Samples 1–2 are studied with the FIGIFIGO experimental apparatus only. The natural sample (1) is
146 abundant with coarse, millimeter-sized particles. Unfortunately, with the CoDuLab apparatus, such
147 particles are too large for a feasible study of their light-scattering behavior at the single-particle level.
148 The problem arises primarily from the aerosol generator, which becomes jammed by such large
149 particles. The sieved volcanic sand (2) consists of particle sizes $< 170 \mu\text{m}$ is used in the CoDuLab
150 experiments, although the signal-to-noise ratios (SNRs) are low. The poor SNRs can be explained as
151 follows: First, many of the sub-millimeter sieved samples remain too large for optimal operation of the
152 aerosol generator. Although the generator operates considerably better with sample (2) than sample (1),
153 the amount of suspended dust remains low leading to weak scattering-signals. Second, due to the large
154 size of the constituent particles, they are much darker in appearance compared to the smaller, micron-
155 sized particles and this can be seen in Fig. 4. Indeed, the milled sample (3) exhibits a brighter
156 appearance in Fig. 4 compared to samples (1) and (2). Optical-microscope images of the samples are
157 included in Fig. 4 to highlight the variability of particle sizes and shapes.

158 To obtain a more detailed view of the particle morphology in the natural sand sample (1), the
159 particles are also examined by scanning electron microscopy (SEM) at various magnifications, see Fig.
160 5. As seen, the particles exhibit a highly irregular and somewhat vesicular morphology. The elemental
161 composition of these particles is analyzed with X-ray spectrometry and the results are presented in
162 Fig. 6. The analysis is repeated for particles of different sizes and it is notable that no significant
163 variation in the chemical composition is found.

164 The size distribution of the milled volcanic sand sample (3) is shown in Fig. 7. The distribution is
165 measured at the IAA CoDuLab with the *MasterSizer2000* instrument by *Malvern Scientific*. Note that
166 the *MasterSizer2000* measures the flux of laser light scattered at a several scattering angles θ near
167 forward-scattering direction. To retrieve information about the particles, it is customary to fit such

168 measurements with the two methods: Fraunhofer-diffraction theory or Mie theory (Bohren & Huffman,
169 1983). As neither of these theories applies well to highly irregular particle shapes in general, the fitting
170 procedure can yield results with error, e.g., with respect to particle size.

171 What emerges from Fig. 7 is that for particle radii $> 0.25\text{--}0.3\ \mu\text{m}$, both approaches reveal a power-
172 law size distribution r^{-n} that can be fit by $n = 3.5$ in the Fraunhofer framework and at $n = 3.2$ in the Mie
173 approach. However, we stress that both approaches assume idealistic targets (spherical particles) and
174 therefore, the results should be taken with caution when applied to the highly irregular particles here.
175 This point will cause some uncertainty in the retrievals of the size distribution that should be taken into
176 account.

177

178 **3. Experimental facilities and measurement details.**

179 **3.1 FIGIFIGO**

180 The Finnish Geodetic Institute goniospectropolarimeter FIGIFIGO (Fig. 2) is designed to measure the
181 reflectance and degree of linear polarization of various surfaces, both in the laboratory and in the field conditions
182 (e.g. Peltoniemi *et al.*, 2015b). A detailed description of the FIGIFIGO can be found in Peltoniemi *et al.*, 2014.
183 In our study, the sample is deposited on the surface by uniform sprinkling particles on a black substrate with a
184 layer of 0.8 - 1 cm thick. The measurements are taken in the principal plane, i.e., when the surface normal lies
185 within the scattering plane and to improve the SNR we repeat the measurements 25 times. To compare phase-
186 angle dependences of the reflectance and the degree of linear polarization of FIGIFIGO with CoDuLab
187 measurements, we present FIGIFIGO results obtained in the waveband $\lambda = 642 - 652\ \text{nm}$ (hereafter $\lambda = 647$
188 nm). The maximum uncertainty, $\sim 3\%$, appears in the polarimetric measurements at some phase angles whereas
189 the average uncertainty in the polarimetric response is $\sim 2\%$. The uncertainty in the measurements of reflectance
190 is noticeably lower compared to that of the polarimetric measurements.

191

192 **3.2 CODULAB**

193 The IAA Cosmic Dust Laboratory (CoDuLab) is designed to measure the light scattering response from
 194 aerosol particles, see Fig. 3. We notice that in the case of irregularly shaped particles, the light-
 195 scattering response can be described by the so-called (4×4) *scattering matrix* or the *Mueller matrix*
 196 consisting of six non-zero elements (see, e.g., Bohren & Huffman 1983):

197

198

$$F = \begin{pmatrix} F_{11} & F_{12} & 0 & 0 \\ F_{12} & F_{22} & 0 & 0 \\ 0 & 0 & F_{33} & F_{34} \\ 0 & 0 & -F_{34} & F_{44} \end{pmatrix}. \quad (1)$$

199

200 Using the CoDuLab facility, one can measure all six non-zero elements over the *scattering angle* θ
 201 range from 3° to 177° at several wavelengths. In our study, we investigate the upper block of non-zero
 202 elements. For a detailed description of the CoDuLab facility refer to (Muñoz *et al.*, 2012).

203 The results presented here are obtained at $\lambda = 647$ nm. In particular, we measure the F_{11} and F_{12}
 204 elements of the scattering matrix for the milled volcanic sand sample (3). The intensity of the scattered
 205 sunlight I and its degree of linear polarization P are defined via the elements of the scattering matrix as
 206 follows: $I \propto F_{11}$, $P = -F_{12} / F_{11}$.

207

208 **4. Results and discussion**209 **4.1 Reflectance and degree of linear polarization**

210 We first investigate the difference in light scattering behavior for the sieved sample deposited on a
211 surface in dry and wet conditions by measuring the reflectance and degree of linear polarization as a
212 function of λ . Spectra for the wet and dry samples at $\theta=170^\circ$ and $\theta=140^\circ$ are shown in Fig. 8. The
213 reflectance of the wet sample is found, on average, to be nearly half of that for the dry sample.
214 Moreover, the shape of the reflectance curve clearly depends on presence of water, which is especially
215 noticeable for λ in the range 500-1000 nm. The reflectance plot demonstrates the highly absorbing
216 property of volcanic sand evidenced by the maximum value being only ~ 0.044 at $\lambda=650$ nm. The
217 strongest reflectance response is observed for the dry sample at $\theta = 170^\circ$. Note, that while the
218 reflectance spectra of this sample differs unambiguously at the two scattering angles ($\theta=170^\circ$ and
219 $\theta=140^\circ$), a similar difference for the wet sample is less in magnitude.

220 In contrast to the reflectance spectra, the curve shapes and scattering response of the polarization
221 spectra are not as sensitive to water content. As shown later, however, a discrimination between wet
222 and dry particles is easier at smaller θ . On the other hand, the degree of linear polarization decreases as
223 the scattering angle grows. This is better seen in the angular dependence of the polarization in the wet
224 and dry samples shown in Fig. 9, where the measurements are taken at $\lambda = 647$ nm. We see that the
225 reflectance of the wet sample (blue curve) decreases considerably whereas the polarimetric response
226 becomes noisier. In the latter case, however, the polarimetric response for the wet sample (blue curve)
227 is higher compared to the dry sample (black curve). The difference between the dry and wet samples is
228 best seen at side scattering, $\theta \sim 90^\circ$. Also, the increase of uncertainty in our measurements can be
229 explained by the continuous evaporation of water during the measurements. To minimize the effect due
230 to evaporation, we replenish the water content in the sample several times during the course of the
231 experiment with water atomizer.

232 Particle size is a dominate factor affecting the light-scattering behavior of a sample, which is
233 illustrated in Fig. 10 for reflectance and polarization at $\lambda = 647$ nm. Here, the natural and milled
234 volcanic sand samples (1) and (3), respectively, are illuminated at $\theta=148^\circ$. Near the backscattering
235 direction, i.e., $\theta \rightarrow 180^\circ$, the reflectance of the milled sample appears to be considerably higher than
236 that of the natural sample. This change is consistent with the so-called *Umov effect* or *Umov law*, which
237 is the inverse correlation between reflectance near backscattering, i.e., geometric albedo, and the
238 maximum value that the degree of linear polarization may acquire, e.g., see Shkuratov & Opanasenko
239 1992; Zubko *et al.* 2016. According to the Umov effect, greater polarization is expected from the
240 natural sand compared to the milled sand. Indeed, the maximum degree of linear polarization of the
241 milled sample is ~ 2.5 times less than that for the natural sample. Also note, that the value of negative
242 polarization near the backscattering direction is greater for the milled sample. The Umov effect can be
243 seen for the near-backscattering reflectance and polarization maximum for the dry and wet sieved
244 samples presented in Fig. 9.

245 Comparing the reflectance of the dry sieved samples shown in Fig. 9 with the reflectance for the
246 natural and milled samples in Fig. 10, one finds that the reflectance of the sieved sample is greater than
247 the natural sand and less than the milled sand. Correspondingly, the polarization of the sieved sample is
248 smaller than for the natural sand and greater than the milled sand.

249 Comparative analysis of the light-scattering behavior for deposited particles and the same type of
250 particles suspended in air as an “optically thin cloud,” i.e., as an aerosol, can provide important
251 information needed for the interpretation of observations of atmosphere and underlying terrain. The
252 milled volcanic sand is measured in both scenarios, i.e., deposited on a surface or as an aerosol, and the
253 results are shown in Fig. 11. Note that for the aerosol, it is not feasible to measure an absolute flux of
254 the scattered light. Therefore, we normalize the reflectance data at $\theta = 90^\circ$. In the FIGIFIGO

255 measurements, the deposited particles are illuminated at $\theta = 52^\circ$ with respect to the surface normal.
256 Due to measurement constraints on the θ range and the increased intensity of scattered light from single
257 particles near the forward-scattering direction, our analysis is limited to the range $60^\circ < \theta < 177^\circ$.

258 In Fig. 11, one can see that the normalized reflectance for the aerosol is noticeably stronger for
259 small θ compared to the data for deposited particles. However, the aerosol data also show a decrease
260 and become weaker for $\theta > 90^\circ$. The maximum value of the degree of linear polarization appears
261 greater for deposited particles compared to the aerosol, i.e., $P_{\max} \approx (22.07 \pm 0.93)\%$ at $\theta_{\max} \approx 60^\circ$ and
262 $P_{\max} \approx (18.7 \pm 1.1)\%$ at $\theta_{\max} \approx 100^\circ$, respectively. Although this difference is not large, it is detected
263 with confidence in Fig. 11. For $\theta < 105^\circ$, this finding qualitatively differs from that reported in
264 Shkuratov *et al.* (2007), for example, where ten different samples are investigated including clay,
265 olivine, feldspar, and volcanic ash. All those samples reveal a systematically lower polarization for
266 deposited samples. Our results, however, are in a good agreement with soot measurements by Francis
267 *et al.*, 2011, where polarization measured from surface packed particles considerably exceeds that from
268 the aerosol particles. Notice in Fig. 11 that the negative polarization branch near backscattering for
269 deposited particles appears deeper than the aerosol, which is opposite to the conclusions drawn in
270 Shkuratov *et al.* (2004). This difference could result from specific features of our sample of volcanic
271 sand. It is significant, for example, that our sand is much darker in appearance than any sample used in
272 Shkuratov *et al.* (2004; 2007).

273 The light scattering response for volcanic sand differs considerably from other types of sand
274 such as desert sand, which is obvious from their visual appearance. While volcanic sand is dark in
275 appearance (its geometric albedo is ~ 0.05), desert sands are considerably brighter.

276 In Fig. 12 we plot the normalized reflectance (left) and degree of linear polarization (right) as a
277 function of scattering angle for three different samples: white-clay, milled volcanic-sand, and the ash
278 particles from the Eyjafjallajokull volcano. The light scattering properties of white clay and volcanic
279 ash were studied with CODULAB by Munoz *et al.* in 2011 and Merikallio *et al.* in 2015. Here we
280 present a comparison of the light scattering properties of volcanic sand in this study to the white clay
281 and Eyjafjallajokull volcanic ash samples. White clay mainly consists of illite, kaolinite,
282 montmorillonite, quartz and is an important component of aerosols in the atmosphere. Eyjafjallajokull
283 volcanic ash was collected at 5 km from the source after the April 2010 eruption, where the main
284 constituent is silica, SiO₂. These particles also contain Al₂O₃, CaO, TiO₂, FeO, MgO and Na₂O.

285 As one can see from Fig. 12 there is similarity between the three polarization curves. The
286 refractive index m of the Eyjafjallajokull ash particles could be similar to that in the milled volcanic
287 sand. However, they should differ significantly from that of the white clay, at least with regard to the
288 imaginary part, $\text{Im}(m)$. Nevertheless, the light scattering response of white-clay particles resembles that
289 of the volcanic sand and ash particles. The resemblance could be explained by a difference in size
290 distribution of the white-clay and volcanic sand and ash particles that, by coincidence, compensates the
291 difference in refractive index. The angular profiles of the reflectance at large scattering-angles ($>90^\circ$)
292 clearly differs for the dark samples (volcanic sand and ash) and light samples, i.e., the white clay. Such
293 a feature could be useful in passive remote-sensing of aerosol particles.

294 Fig. 13 compares our results to the polarization measurements obtained for levitated soot-particles
295 by Francis *et al.* (2011). The data adopted from Francis *et al.* is measured at $\lambda = 632.8$ nm from a dense
296 cloud of levitated agglomerated particles of Polymethyl Methacrylate (PMMA), hereafter called the
297 soot sample. The soot particles are micrometer-sized aggregates, where the constituent grains have a
298 diameter of several tens of nm. The maximum polarization of the volcanic sand is about 19%, while the

299 soot is about 25%. Based on this, and considering the Umov law, we can conclude that the near-
300 backscattering reflectance of the soot sample is lower than that of milled volcanic sand.

301

302 **4.2 Constraint of the complex refractive index of volcanic sand**

303 An advantage of our study with single-scattering particles is that interpretation data does not involve
304 common complications due multiple scattering. We can develop a quantitative model describing the
305 single-scattering particles based on a numerically exact solution of the Maxwell equations, although
306 this cannot be done here for the deposited particles. The ultimate goal of such modeling is retrieval of
307 the microphysical properties of the particles.

308 In general, light scattering by submicron and micron-sized particles is dependent on their size
309 distribution, shape, and complex refractive index (m). However, Zubko *et al.* (2015) show that in the
310 case of highly irregular particles, the effect of size distribution and m on the light scattering behavior
311 dominates the effects of particle shape. Furthermore, the size distribution of the milled volcanic sand is
312 constrained by the *MasterSizer2000* measurements (Fig. 7) and this allows us to estimate m for the
313 volcanic sand with the light-scattering model.

314 Specifically, we model the angular profiles of the scattered intensity I and degree of linear
315 polarization P for the milled volcanic-sand particles using the so-called *agglomerated debris particles*
316 method (Zubko, 2015, Zubko *et al.* 2015b). Such particles have a disordered morphology with a
317 packing density of the constituent material being ~ 0.236 . Six examples of the agglomerated debris
318 particles are shown in Fig. 14, which are generated by systematically damaging a perfect sphere as
319 described in Zubko *et al.* (2013). An notable feature of the model particles is that they reproduce
320 analogous laboratory measurements of a variety of samples similar to those considered here, such as
321 feldspar (Zubko *et al.*, 2013), forsterite (Zubko, 2015), and olivine (Videen *et al.*, 2018). In particular,

322 the model parameters, i.e., the size distribution and m , applied to these analogous measurements closely
323 match the actual microphysical characteristics of the samples.

324 Analysis of satellite data is typically done with spheroidal model-particles, see for example
325 Dubovik et al. However, Dubovik et al. 2006 shows that the use of spheroidal particles could not
326 satisfactorily reproduce laboratory measurements when multiple wavelengths are involved.
327 Furthermore, the microphysical properties retrieved with spheroidal particles do not match the true
328 properties of the feldspar particles (refractive index, size, and aspect-ratio distributions), while
329 agglomerated debris particles is in good quantitative agreement with the true microphysical
330 characteristics of feldspar (Zubko *et al.*, 2013).

331 A particle's light-scattering behavior depends, in part, on the ratio of its radius r to wavelength λ , is
332 commonly called the size parameter $x = 2\pi r/\lambda$ (Bohren & Huffman 1983). In application to an
333 irregularly shaped particle, we assign r to a sphere that circumscribes the model particle used. Then, we
334 compute the relevant light-scattering quantities using agglomerated debris particles for $1 < x < 32$ with
335 the *discrete dipole approximation* (DDA). The DDA is a flexible technique designed for numerical
336 simulation of light scattering by particles with an arbitrary shape (Yurkin *et al.* 2007). In the DDA
337 framework, the particle is replaced by a set of cubic cells that reproduces the shape and internal
338 structure, where the size of the cells d is sufficiently small compared to λ . As demonstrated in Zubko *et*
339 *al.* (2010), the DDA yields robust numerical results for $2\pi d|m|/\lambda \leq 1$. Each cell is then approximated by
340 an electric dipole and, thus, the integral equation describing interaction of an electromagnetic wave
341 with the particle is transformed into a system of linear algebraic equations. This system of equations is
342 then solved via an iterative method. In order to comply with the discretization criterion for d above, we
343 consider two cases for each agglomerated debris particle: $64 \times 64 \times 64$ cells and $128 \times 128 \times 128$ cells.
344 The former is used when $x \leq 15$ and the latter when $x > 15$. The size parameter is varied in steps of Δx

345 = 1 for $1 < x < 15$ and $\Delta x = 2$ for $16 < x < 32$. Given that $\lambda = 647$ nm in our study, this size-parameter
346 range corresponds to a particle-size range $0.1 \mu\text{m} < r < 3.3 \mu\text{m}$. As demonstrated in Zubko *et al.* (2013),
347 Zubko (2015), and Videen *et al.* (2018), such a range is sufficient to reproduce the light-scattering
348 response in a polydisperse system exhibiting a power-law size distribution with an exponent of $n \geq 2.9$.

349 To investigate the dependence on m , we apply the DDA to agglomerated debris particles at 46
350 values of m , with real and imaginary parts spanning the ranges $1.1 < \text{Re}(m) < 2.43$ and $0 < \text{Im}(m) < 1$,
351 respectively. For every pair (x, m) we average the light-scattering response over a minimum of 500
352 random shapes to ensure a statistically reliable result. We also perform size averaging using a power-
353 law distribution r^{-n} over the full range of r considered. Initial values for n are inferred from Fig. 7, i.e.,
354 $n = 3.2$ and 3.5 . However, we do not consider these as precisely known values. Instead, we assume a
355 degree of variation of ± 0.5 , which recognizes the uncertainty inherent to the size distribution
356 measurements with the *MasterSizer 2000* instrument.

357 We investigate all the available refractive indices, searching for the best fit to the maximum value of
358 the degree of linear polarization $P_{\text{max}} \approx (18.7 \pm 1.1)\%$ found for the milled-sand sample at $\theta = 100^\circ$.
359 When such fit is possible, we then compare the entire angular profiles of I and P measured for the
360 given sample with that from the DDA model applied to agglomerated debris particles (Zubko *et al.*,
361 2013; Zubko, 2015; Videen *et al.*, 2018). As Fig. 14 shows, the best fit for $\lambda = 647$ nm is obtained for
362 $m = 1.6 + 0.01i$ and $n = 2.85$. As one can see, the intensity is reproduced well for all θ , whereas the
363 degree of linear polarization tends to agree less near backscattering ($\theta > 140^\circ$) where the phenomenon
364 of negative polarization is observed (i.e., $I_{\perp} < I_{\parallel}$). The same qualitative behavior is seen for a feldspar
365 particle (Zubko *et al.*, 2013), although the difference is smaller. Overall, the agglomerated debris
366 particle model in other work closely matches the true microphysical properties of the measured particle

367 (Zubko *et al.*, 2013; Zubko, 2015; Videen *et al.*, 2018). Such performance of the model lends
368 confidence to our conclusion in Fig. 14 that $m = 1.6 + 0.01i$ for the volcanic sand at $\lambda = 647$ nm.

369 Finally, consider the question of how the inferred material absorption, i.e., $\text{Im}(m) = 0.01$,
370 corresponds to the dark appearance of the milled volcanic sand, having a reflectance ~ 0.1 near
371 backscattering $\theta = 175^\circ$ and presumably ~ 0.12 at $\theta = 180^\circ$ (see Fig. 11). We draw attention to previous
372 laboratory measurements of m in powdered kerogen type-II reported by Khare *et al.* (1990). In
373 particular, for the red part of the spectrum, a similar value for $\text{Im}(m)$ is found, $\text{Im}(m) \approx 0.012$, whereas
374 the powder is described as having the dark appearance. Thus, our finding that $\text{Im}(m) = 0.01$ for the
375 volcanic sand agrees well with the visual appearance of the sand deposited on a surface.

376

377 5. Conclusions

378 Our study of the light-scattering behavior of Icelandic volcanic sand achieves a quantitative
379 characterization of this important material. The reflectance and polarization deposited sand strongly
380 depends on the particle size-distribution. According to the Umov law, the maximum of the polarization
381 degree encodes information on the material's optical absorption and reflectance. This effect is
382 demonstrated for the three samples of volcanic sand containing particles with different size
383 distributions. The degree of linear polarization differs by nearly a factor of three between the milled
384 and natural-sand samples whereas the polarization seen for the sieved sample is smaller than the natural
385 sand and greater than the milled sand. However, the water added to the sieved sand increases its
386 polarimetric response considerably, so that at some scattering angles the response is nearly the same as
387 the natural sand, which consists of larger particles. This observation may have important implications
388 for remote-sensing observations of regions with such sand present.

389 Our comparative analysis of the reflectance and polarization response of particles suspended as an
390 aerosol with those deposited on a surface reveal:

- 391 (1) The normalized reflectance of light scattered by the aerosols is noticeably stronger at small
392 scattering-angles compared to that of the deposited particles.
- 393 (2) The positive degree of linear polarization for the aerosols is greater than for the deposited
394 particles for $90^\circ < \theta < 160^\circ$.
- 395 (3) The maximum polarization is as large as $P_{\max} \approx 22\%$ occurring at $\theta_{\max} \approx 60^\circ$ for deposited
396 particles, and $P_{\max} \approx 19\%$ at $\theta_{\max} \approx 100^\circ$ for the aerosol particles.
- 397 (4) The polarization response from the aerosol and deposited particles becomes similar at $\theta = 95^\circ$.
- 398 (5) The negative polarization branch of deposited particles is deeper than that of the aerosol.

399 Finally, based on discrete-dipole modeling of the reflectance and degree of linear polarization we
400 estimate the refractive index of the Icelandic volcanic sand to be $m = 1.6 + 0.01i$ at $\lambda = 647$ nm.

401

402 **Acknowledgments**

403 This research was partially supported by the Academy of Finland Project no. 260027 and the COST
404 Action MP1104 “Polarization as a tool to study the Solar System and beyond”. NZ acknowledges
405 Magnus Ehrnrooth Foundation for the research travel support. We thank P. Dagsson Waldhauserová, O.
406 Arnalds, A. Virkkula, O. Meinander, and J. Svensson for their help obtaining the samples and for
407 relevant discussions. We acknowledge the use of imagery provided by services from NASA's Global
408 Imagery Browse Services (GIBS), part of NASA's Earth Observing System Data and Information
409 System (EOSDIS). We also would like to thank reviewers for their constructive reviews.

410

411 **References**

412

413 **Arnalds, O., Gísladóttir, F.O., Sigurjónsson, H., 2001.** Sandy deserts of Iceland: an overview. *Journal*
414 *of Arid Environments* 47:359–371. <https://doi.org/10.1006/jare.2000.0680>

415 **Arnalds, O., Thorarinsdóttir, E.F., Thorsson, J., Waldhauserova, P.D., Agustsdóttir, A.M., 2013.** An
416 extreme wind erosion event of the fresh Eyjafjallajökull 2010 volcanic ash. *Scientific Reports* 3.
417 <https://doi.org/10.1038/srep01257>

418 **Arnalds, O., 2015.** *The Soils of Iceland, World Soils Book Series.* Springer Netherlands.
419 <https://doi.org/10.1007/978-94-017-9621-7>
420 **Kok, J.F., Parteli, E.J.R., Michaels, T.I., Karam, D.B., 2012.**
421 The physics of wind-blown sand and dust. *Reports on Progress in Physics* 75, 106901.
422 <https://doi.org/10.1088/0034-4885/75/10/106901>

422 **Baratoux, D., Mangold, N., Arnalds, O., Bardintzeff, J.-M., Platevoët, B., Grégoire, M., Pinet, P.,**
423 **2011.** Volcanic sands of Iceland – Diverse origins of aeolian sand deposits revealed at Dyngjusandur
424 and Lambahraun. *Earth Surface Processes and Landforms* 36, 1789–1808.
425 <https://doi.org/10.1002/esp.2201>

426 **Boucher, O., D. Randall, P. Artaxo, C. Bretherton, G. Feingold, P. Forster, V.-M. Kerminen, Y. Kondo,**
427 **H. Liao, U. Lohmann, P. Rasch, S.K. Satheesh, S. Sherwood, B. Stevens and X.Y. Zhang, 2013:**
428 **Clouds and Aerosols.** In: *Climate Change 2013: The Physical Science Basis. Contribution of Working*
429 *Group I to the Fifth Assessment Report of the Intergovernmental Panel on Climate Change* [Stocker,
430 T.F., D. Qin, G.-K. Plattner, M. Tignor, S.K. Allen, J. Boschung, A. Nauels, Y. Xia, V. Bex and P.M.
431 Midgley (eds.)]. Cambridge University Press, Cambridge, United Kingdom and New York, NY, USA.

- 432 Bohren, C. F., Huffman, D. R., 1983. Absorption and Scattering of Light by Small Particles. Wiley,
433 New York.
- 434 **Dagsson-Waldhauserova, P.,** Magnúsdóttir, A., Ólafsson, H., Arnalds, O., 2016. The Spatial
435 Variation of Dust Particulate Matter Concentrations during Two Icelandic Dust Storms in 2015.
436 *Atmosphere* 7, 77. <https://doi.org/10.3390/atmos7060077>
- 437 **Dubovik, O.,** A. Sinyuk, T. Lapyonok, B.N. Holben, M. Mishchenko, P. Yang, T.F. Eck, H. Volten, O.
438 Muñoz, B. Veihelmann, W.J. van der Zande, J.-F. Leon, M. Sorokin, and I. Slutsker, 2006: Application
439 of spheroid models to account for aerosol particle nonsphericity in remote sensing of desert dust. *J.*
440 *Geophys. Res.*, 111, D11208, doi:10.1029/2005JD006619.
- 441 **Dubovik, O.,** Li, Z. Mishchenko, M.I. et al., 2019. *Journal of Quantitative Spectroscopy & Radiative*
442 *Transfer*, 224, 474–511
- 443 **Edgett, K.S. & Lancaster, N. ,** 1993. Volcaniclastic aeolian dunes: terrestrial examples and application
444 to martian sands. *Journal of Arid Environments*, 25: 271–297.
- 445 **Groot Zwaaftink, C.D.,** Arnalds, Ó., Dagsson-Waldhauserova, P., Eckhardt, S., Prospero, J.M., Stohl,
446 A., 2017. Temporal and spatial variability of Icelandic dust emissions and atmospheric transport.
447 *Atmospheric Chemistry and Physics* 17, 10865–10878. <https://doi.org/10.5194/acp-17-10865-2017>
- 448 **Hadamcik, E.,** 2002. Polarization of Light Scattered by Fluffy Particles (PROGRA2 Experiment).
449 *Icarus* 155, 497–508. <https://doi.org/10.1006/icar.2001.6732>
- 450 **Herman M.,** 2005. Aerosol remote sensing from POLDER/ADEOS over the ocean: improved retrieval
451 using a nonspherical particle model. *J. Geophys. Res.*, 110:D10S02. doi: 10.1029/2004JD004798 .

- 452 Kahn, R. A., and Gaitley, B. J. (2015), An analysis of global aerosol type as retrieved by MISR. J.
453 Geophys. Res. Atmos., 120, 4248– 4281. doi: 10.1002/2015JD023322.
- 454 **Khare**, B. N., Thompson, W. R., Sagan, C., Arakawa, E. T., Meisse C., & Gilmour, I., 1990. Optical
455 constants of kerogen from 0.15 to 40 μm : comparison with meteoritic organics. In: Proceedings of
456 Lunar and Planetary Science Conference XXI, 627–628.
- 457 **Meinander**, O., Kontu, A., Virkkula, A., Arola, A., Backman, L., Dagsson-Waldhauserová, P.,
458 Järvinen, O., Manninen, T., Svensson, J., de Leeuw, G., Leppäranta, M., 2014. Brief communication:
459 Light-absorbing impurities can reduce the density of melting snow. *The Cryosphere* 8, 991–995.
460 <https://doi.org/10.5194/tc-8-991-2014>
- 461 **Munro**, R., Lang, R., Klaes, D., Poli, G., Retscher, C., Lindstrot, R., et al., 2016. The GOME-2
462 instrument on the Metop series of satellites: instrument design, calibration, and level 1 data processing
463 –an overview. *Atmos. Meas. Tech.*, 9:1279–301. doi: 10.5194/amt- 9- 1279- 2016 .
- 464 **Merekallio**, S., Muñoz, O., Sundström, A.-M., Virtanenm T.H. Horttanainen, M., de Leeuw, G.,
465 Nousiainen, T., 2015. Optical modeling of volcanic ash particles using ellipsoids. *Journal of*
466 *Geophysical Research*, 120(9), p. 4102-4116.
- 467 **Muñoz**, O., Volten H., Hoveneir, J.W., veihelmann, B., van der Zande, W.J. Waters, L.B.F.M., Rose,
468 W.I., 2004. Scattering matrices of volcanic ash particles of Mount St. Helens, Redoubt, and Mount
469 Spurr Volcanoes. *Journal of Geophysical Research*, 109, Issue D16, Cite ID D16201.
- 470 **Muñoz**, O., Moreno, F., Guirado, D., Ramos, J.L., Volten. H., Hovenier, J.W. The IAA cosmic dust
471 laboratory: Experimental scattering matrices of clay particles. *Icarus*, 211 (2011) 894-900.

- 472 **Muñoz**, O., Moreno, F., Guirado, D., Dabrowska, D.D., Volten, H., Hovenier, J.W., 2012. The
473 Amsterdam–Granada Light Scattering Database. *Journal of Quantitative Spectroscopy and Radiative*
474 *Transfer* 113, 565–574. <https://doi.org/10.1016/j.jqsrt.2012.01.014>
- 475 **Peltoniemi**, J., Hakala, T., Suomalainen, J., Puttonen, E., 2009. Polarised bidirectional reflectance
476 factor measurements from soil, stones, and snow. *Journal of Quantitative Spectroscopy and Radiative*
477 *Transfer* 110, 1940–1953. <https://doi.org/10.1016/j.jqsrt.2009.04.008>
- 478 **Peltoniemi**, J.I., Hakala, T., Suomalainen, J., Honkavaara, E., Markelin, L., Gritsevich, M., Eskelinen,
479 J., Jaanson, P., Ikonen, E., 2014. Technical notes: A detailed study for the provision of measurement
480 uncertainty and traceability for goniospectrometers. *Journal of Quantitative Spectroscopy and*
481 *Radiative Transfer* 146, 376–390. <https://doi.org/10.1016/j.jqsrt.2014.04.011>
- 482 **Peltoniemi**, J.I., Gritsevich, M., Hakala, T., Dagsson-Waldhauserová, P., Arnalds, Ó., Anttila, K.,
483 Hannula, H.-R., Kivekäs, N., Lihavainen, H., Meinander, O., Svensson, J., Virkkula, A., de Leeuw, G.,
484 2015a. Soot on Snow experiment: bidirectional reflectance factor measurements of contaminated snow.
485 *The Cryosphere* 9, 2323–2337. <https://doi.org/10.5194/tc-9-2323-2015>
- 486 **Peltoniemi**, J.I., Gritsevich, M., Puttonen, E., 2015b. Reflectance and polarization characteristics of
487 various vegetation types // Springer Praxis Books, *Light Scattering and Radiative Transfer, Light*
488 *Scattering Reviews* 9, pp. 257-294, http://dx.doi.org/10.1007/978-3-642-37985-7_7
- 489 **Prospero**, J. M., Bullard, J. N., Hodgkins, R. 2012. High-latitude dust over the north atlantic: inputs
490 from icelandic proglacial dust storms. *Science*, 335, issue 6072, pp. 1078-1082
491 <https://doi.org/10.1126/science.1217447>
- 492 **Qian**, Y., Gustafson, W.I., Jr., Leung, L.R., Ghan, S.J., 2009. Effects of soot-induced snow albedo
493 change on snowpack and hydrological cycle in western United States based on Weather Research and

- 494 Forecasting chemistry and regional climate simulations. *Journal of Geophysical Research* 114.
495 <https://doi.org/10.1029/2008jd011039>
- 496 **Shkuratov**, Yu.G., Opanasenko, N.V., 1992. Polarimetric and photometric properties of the moon:
497 Telescope observation and laboratory simulation. II – The positive polarization. *Icarus* 99, 468–484;
498 [https://doi.org/10.1016/0019-1035\(92\)90161-Y](https://doi.org/10.1016/0019-1035(92)90161-Y)
- 499 **Shkuratov**, Y., Ovcharenko, A., Zubko, E., Volten, H., Muñoz, O., Videen, G., 2004. The negative
500 polarization of light scattered from particulate surfaces and of independently scattering particles.
501 *Journal of Quantitative Spectroscopy and Radiative Transfer* 88, 267–284.
502 <https://doi.org/10.1016/j.jqsrt.2004.03.029>
- 503 **Shkuratov**, Yu., Bondarenko, S., Kaydash, V., Videen, G., Muñoz, O., Volten, H., 2007. Photometry
504 and polarimetry of particulate surfaces and aerosol particles over a wide range of phase angles. *J. Quant.*
505 *Spectrosc. Radiat. Transfer* 106, 487–508; <https://doi.org/10.1016/j.jqsrt.2007.01.031>
- 506 **Sinyuk**, A., Dubovik, O., Holben, B., Eck, T.F., Bréon, F-M, Martonchik, J., et al., 2007. Simultaneous
507 retrieval of aerosol and surface properties from a combination of AERONET and satellite data. *Remote*
508 *Sens. Environ.*;107:90–108.
509 <https://doi.org/10.1016/j.rse.2006.07.022>
- 510 **Sun**, Z., Zhang, J., Tong, Z., Zhao, Y., 2014. Particle size effects on the reflectance and negative
511 polarization of light backscattered from natural surface particulate medium: Soil and sand. *Journal of*
512 *Quantitative Spectroscopy and Radiative Transfer* 133, 1–12.
513 <https://doi.org/10.1016/j.jqsrt.2013.03.013>

- 514 **Tao**, M., Chen, L., Wang, Z., Wang, J., Che, H., Xu, X., ... Hou, C. (2017). Evaluation of MODIS
515 Deep Blue aerosol algorithm in desert region of East Asia: Ground validation and intercomparison.
516 Journal Geophysical Research: Atmospheres, 122, 10, 357–10, 368.
517 <https://doi.org/10.1002/2017JD026976>
- 518 **Videen**, G., Zubko, E., Arnold, J.A., MacCall, B., Weinberger, A.J., Shkuratov, Yu., & Muñoz, O.,
519 2018. On the interpolation of light-scattering responses from irregularly shaped particles. J. Quant.
520 Spectrosc. Radiat. Transfer, 211, 123–128 ; <https://doi.org/10.1016/j.jqsrt.2018.03.009>
- 521 **Wilkman** O., Gritsevich M., Zubko N., Peltoniemi J., Muinonen K., 2016. Photometric modelling for
522 laboratory measurements of dark volcanic sand // Journal of Quantitative Spectroscopy and Radiative
523 Transfer 185, 37–47 <http://dx.doi.org/10.1016/j.jqsrt.2016.08.013>
- 524 **Winker**, D.M. Vaughan, M.A., Omar, A., Hu, Y., Powell, K.A., Liu, Z., et al., 2009. Overview of the
525 CALIPSO mission and CALIOP data processing algorithms. J Atmos Ocean Technol, 26 :2310–23.
526 Doi : 10.1175/2009JTECHA1281.1 .
- 527 **Wittmann**, M., Groot Zwaafink, C.D., Steffensen Schmidt, L., Guðmundsson, S., Pálsson, F., Arnalds,
528 O., Björnsson, H., Thorsteinsson, T., Stohl, A., 2017. Impact of dust deposition on the albedo of
529 Vatnajökull ice cap, Iceland. The Cryosphere 11, 741–754. <https://doi.org/10.5194/tc-11-741-2017>
- 530 **Zubko**, E., Petrov, D., Grynko, Ye., Shkuratov, Yu., Okamoto, H., Muinonen, K., Nousiainen, T.,
531 Kimura, H., Yamamoto, T., & Videen, G., 2010. Validity criteria of the discrete dipole approximation.
532 Appl. Opt., 49, 1267–1279; <https://doi.org/10.1364/AO.49.001267>
- 533 **Zubko**, E., Muinonen, K., Muñoz, O., Nousiainen, T., Shkuratov, Yu., Sun, W., & Videen, G., 2013.
534 Light scattering by feldspar particles: comparison of model agglomerate debris particles with

535 laboratory samples. *J. Quant. Spectrosc. Radiat. Transfer*, 131, 175–187;
536 <https://doi.org/10.1016/j.jqsrt.2013.01.017>

537 **Zubko**, E., 2015. Modeling light scattering by forsterite particles. *Opt. Lett.*, 40, 1204–1207;
538 <https://doi.org/10.1364/OL.40.001204>

539 **Zubko**, E., Shkuratov, Yu., & Videen, G., 2015b. Effect of morphology on light scattering by
540 agglomerates. *J. Quant. Spectrosc. Radiat. Transfer*, 150, 42–54 ;
541 <https://doi.org/10.1016/j.jqsrt.2014.06.023>

542 **Zubko**, N., Gritsevich, M., Zubko, E., Hakala, T., Peltoniemi, J.I., 2016. Optical measurements of
543 chemically heterogeneous particulate surfaces. *Journal of Quantitative Spectroscopy and Radiative*
544 *Transfer* 178, 422–431. <https://doi.org/10.1016/j.jqsrt.2015.12.010>

545

546 **Figures**

547

548 **Figure 1**

549 Satellite image of Iceland obtained with MODIS (Blue Marble from August 2004). Enlarged image of
550 the selected area is taken from MODIS 08.07.2009).

551



552

553

554

555

556

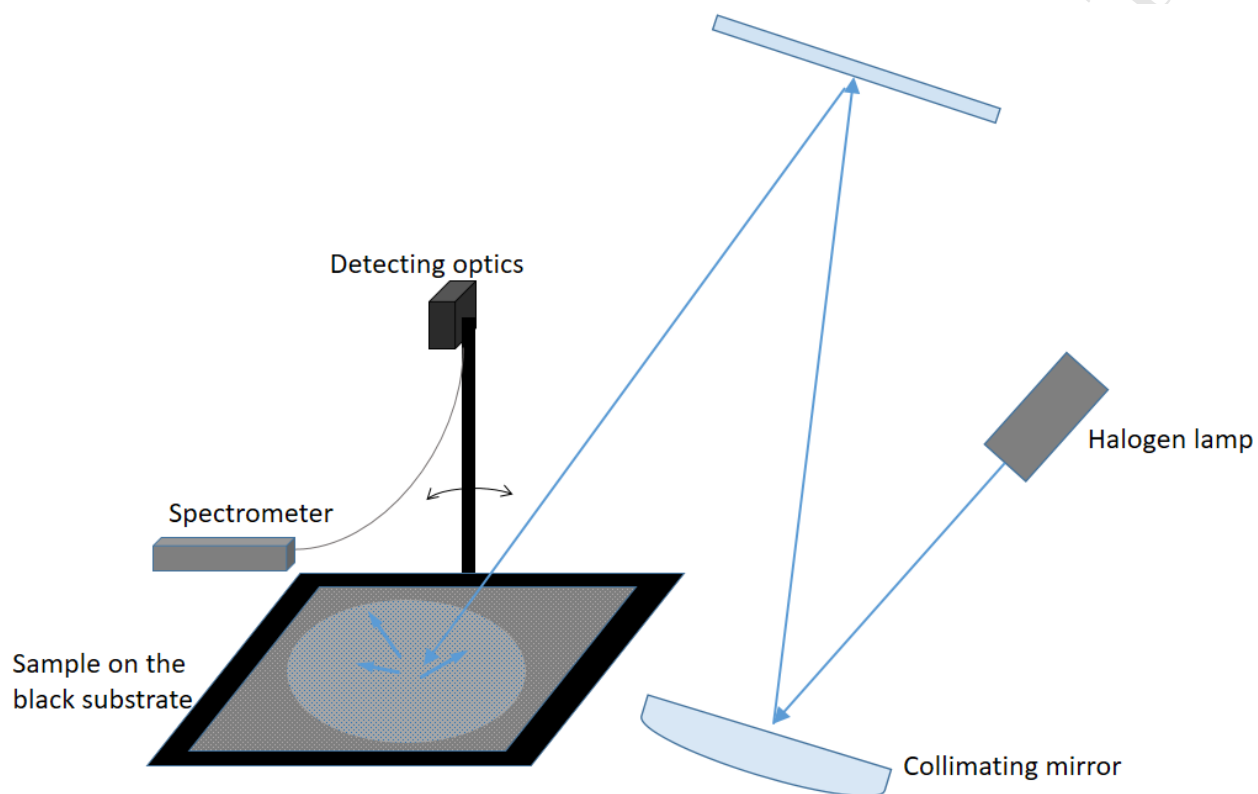
557 **Figure 2**

558

559 Scheme of Finnish Geospatial Research Institute goniospectropolarimeter FIGIFIGO setup

560

561



562

563

564

565 **Figure 3**

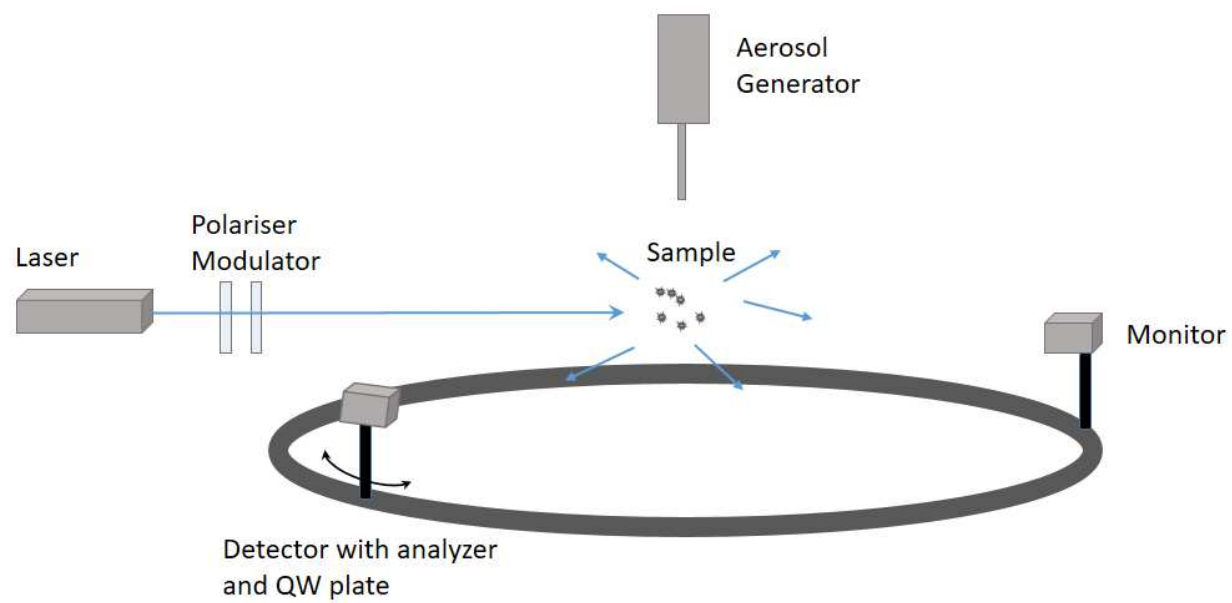
566

567 Scheme of IAA Cosmic Dust Laboratory setup

568

569

570



571

572

573

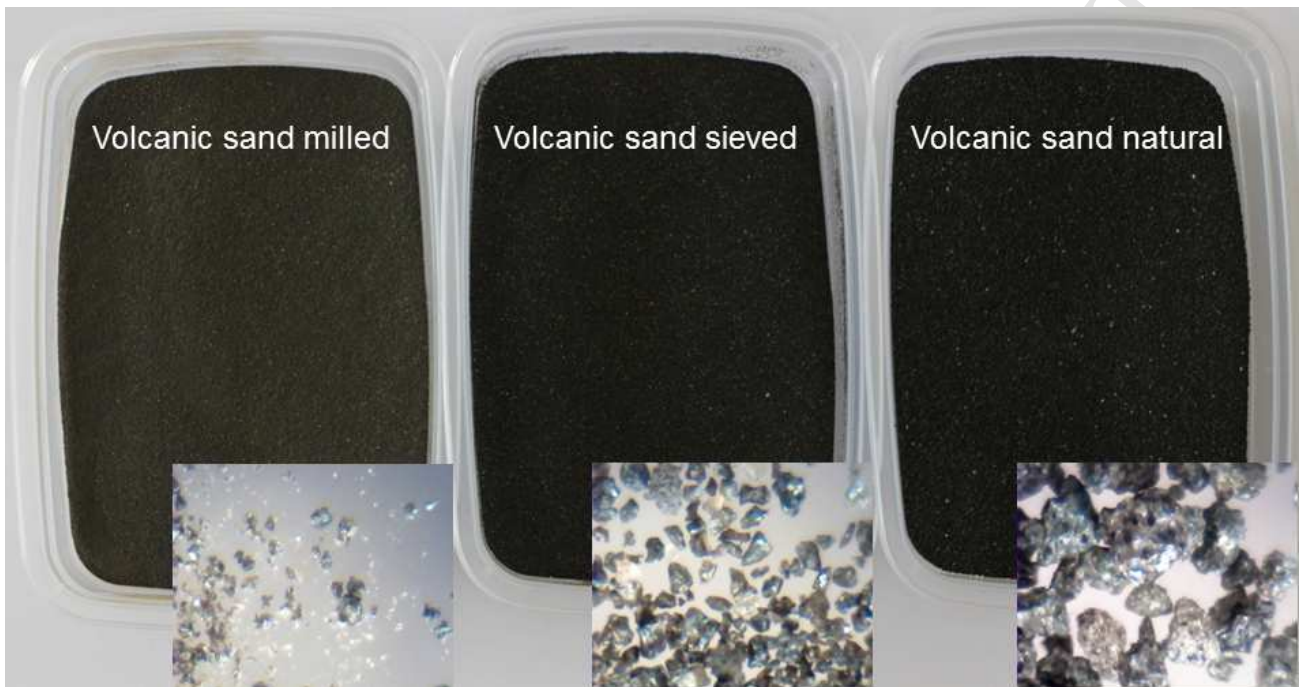
574

575 **Figure 4**

576

577 Appearance of milled, sieved, and natural volcanic sand samples along with optical-microscope images
578 of the same samples.

579



580

581

582

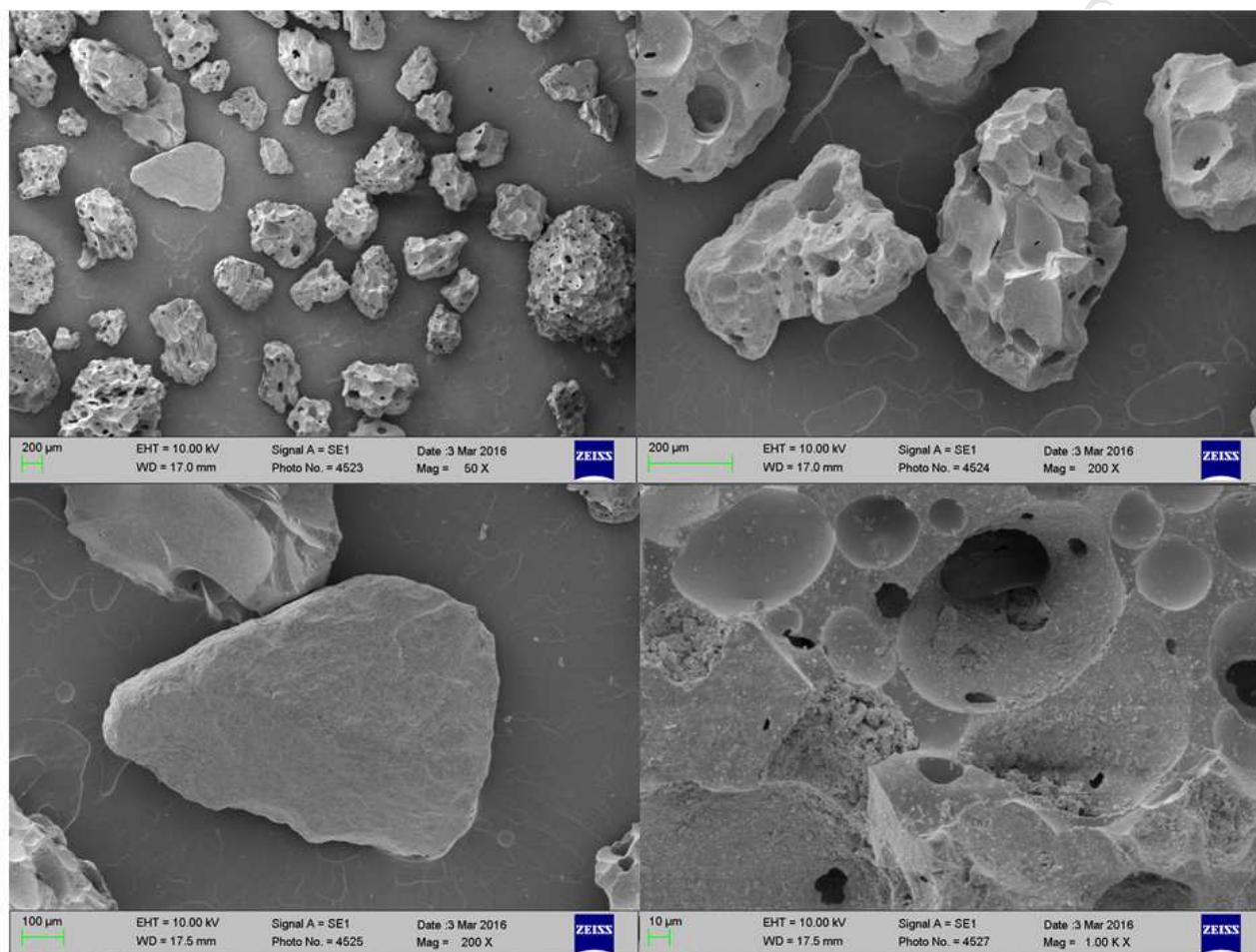
583

584 **Figure 5**

585

586 Scanning electron microscopic images of the natural sample

587



588

589

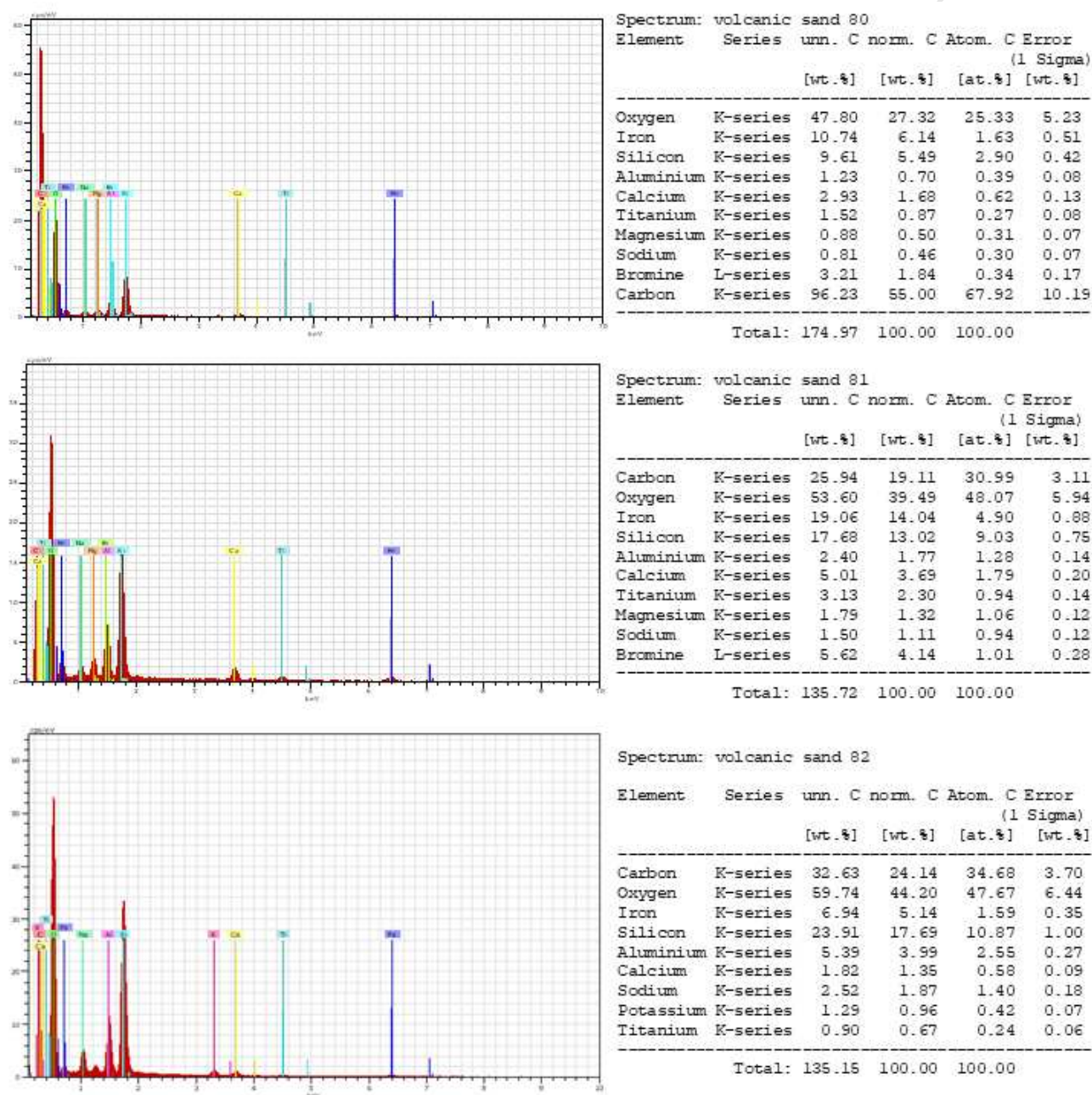
590

591 **Figure 6**

592

593 Element composition of natural volcanic sand particles analyzed with the X-ray spectrometry

594



595

596

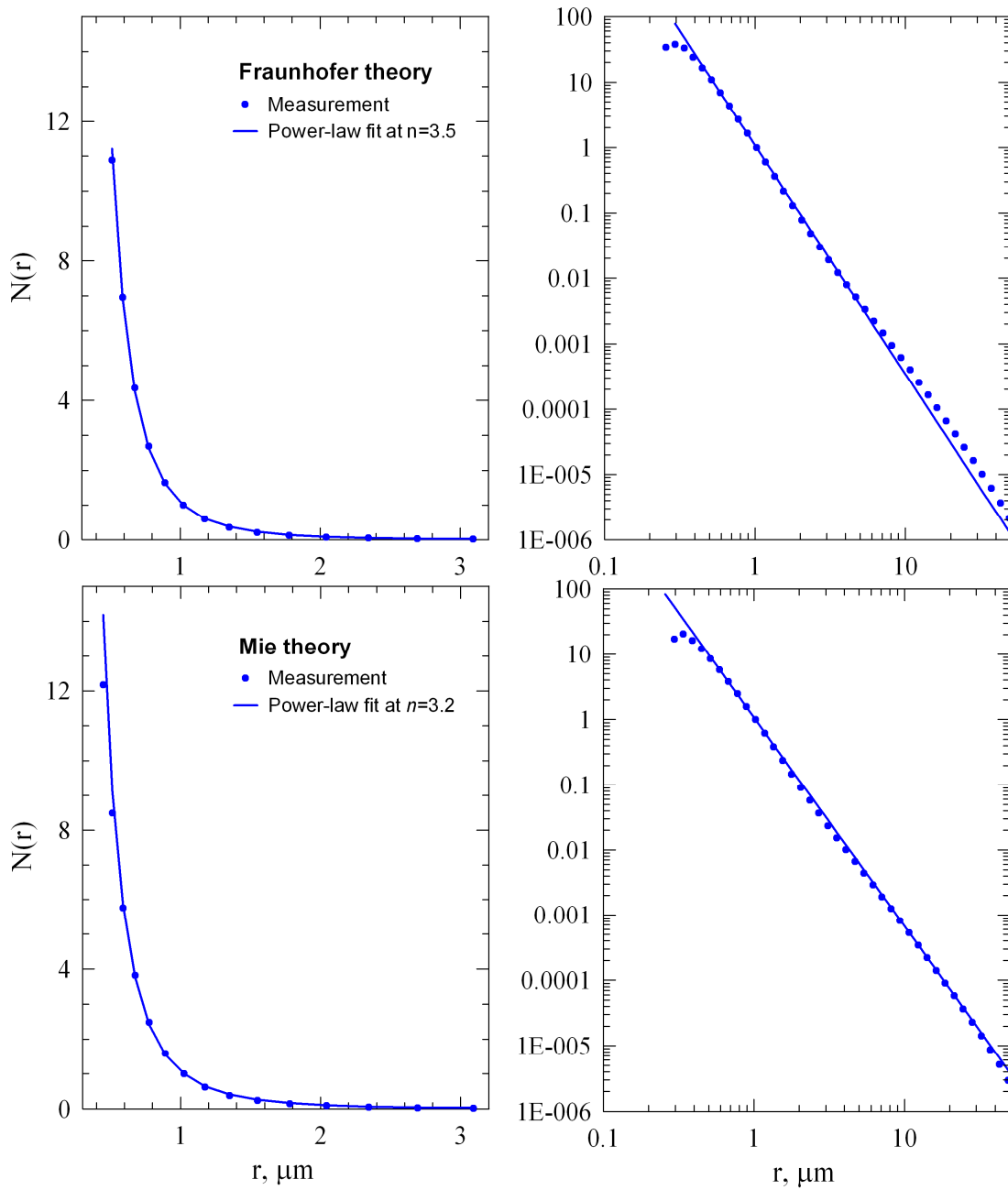
597

598 **Figure 7**

599

600 Size distribution of the milled volcanic sand particles on linear scale on the right and log scale on the left.

602



603

604

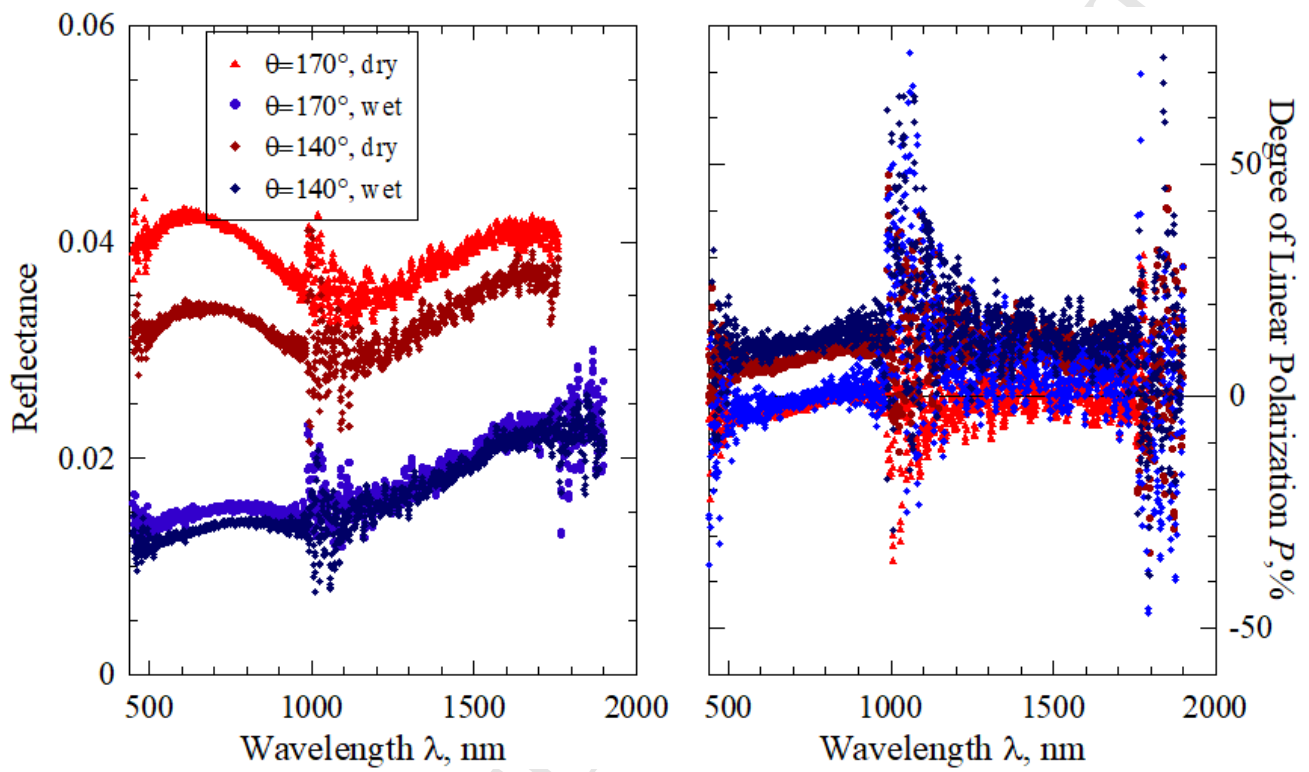
605

606 **Figure 8**

607

608 Reflectance and degree of linear polarization as function of wavelength of sieved wet and dry volcanic
609 sand particles deposited on the surface.

610



611

612

613

614

615 **Figure 9**

616

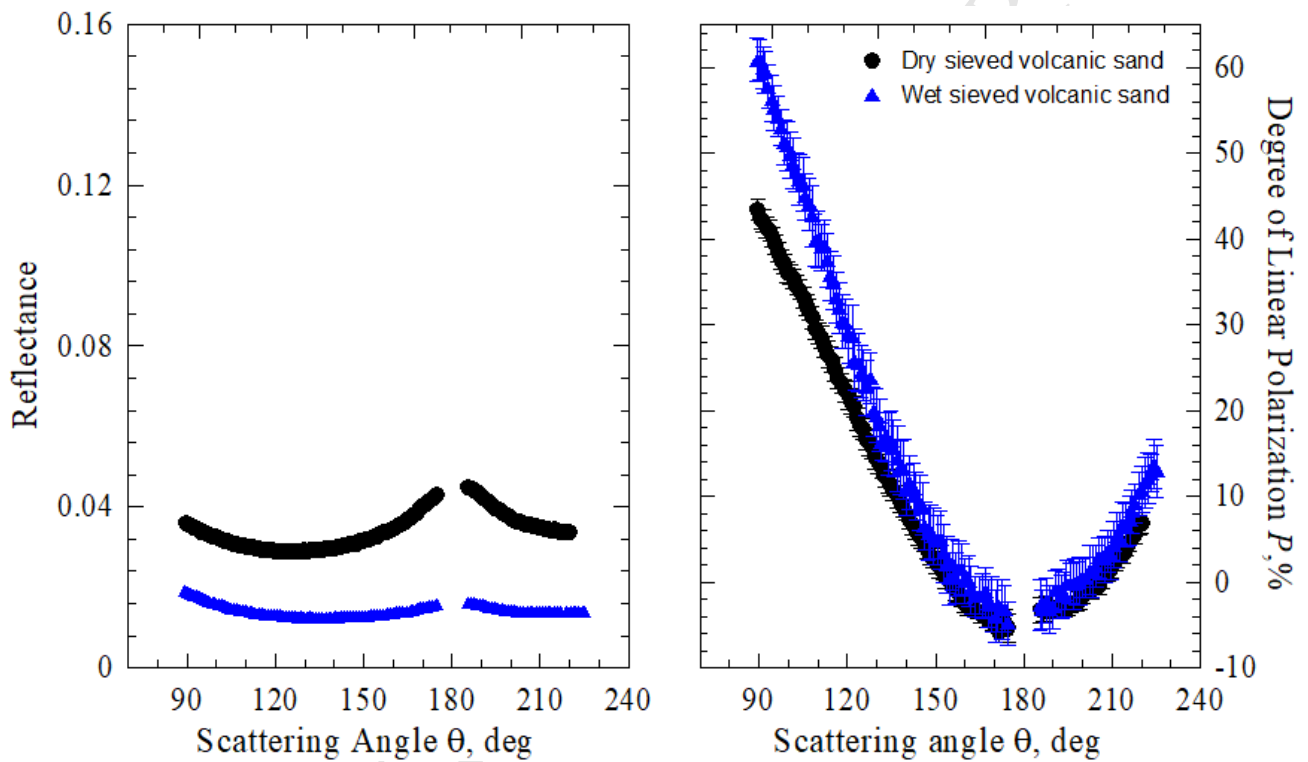
617 Reflectance and degree of linear polarization of the dry and wet sieved volcanic sand as a function of
618 scattering angle at wavelength of 647 nm

619

620

621

622



623

624

625 **Figure 10**

626

627 Reflectance and degree of linear polarization of the dry natural and milled volcanic sand as function on
628 phase angle at wavelength of 647 nm

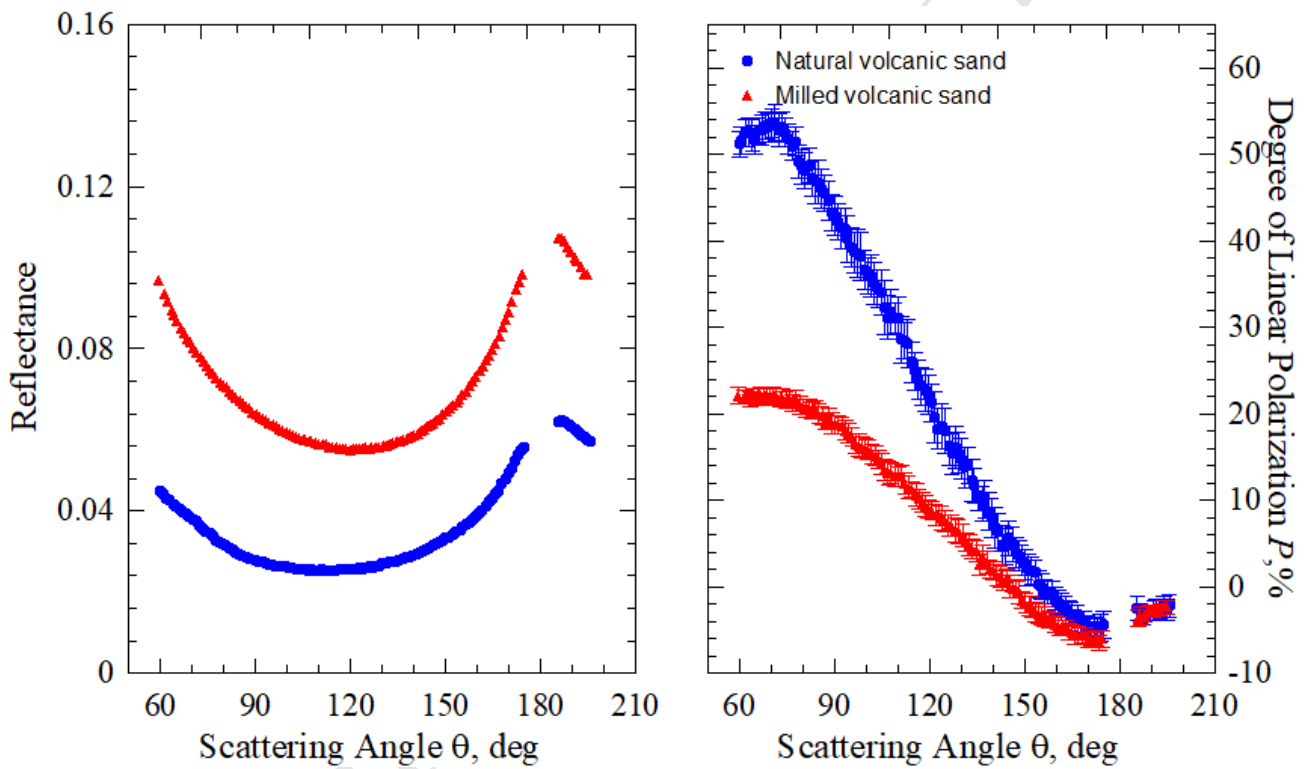
629

630

631

632

633

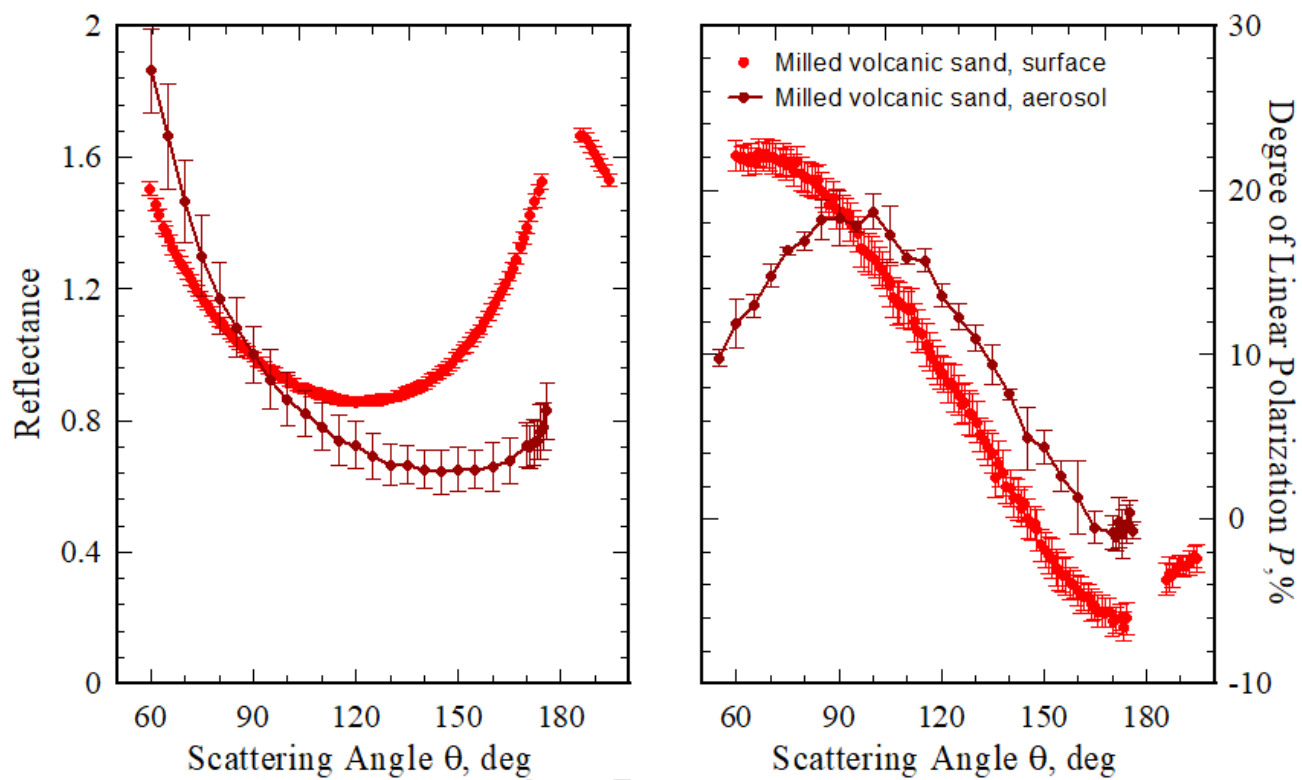


634

635 **Figure 11**

636 The scattering angle dependence of the normalized reflectance and degree of linear polarization
637 obtained for the surface and aerosol of the milled volcanic sand.

638



639

640

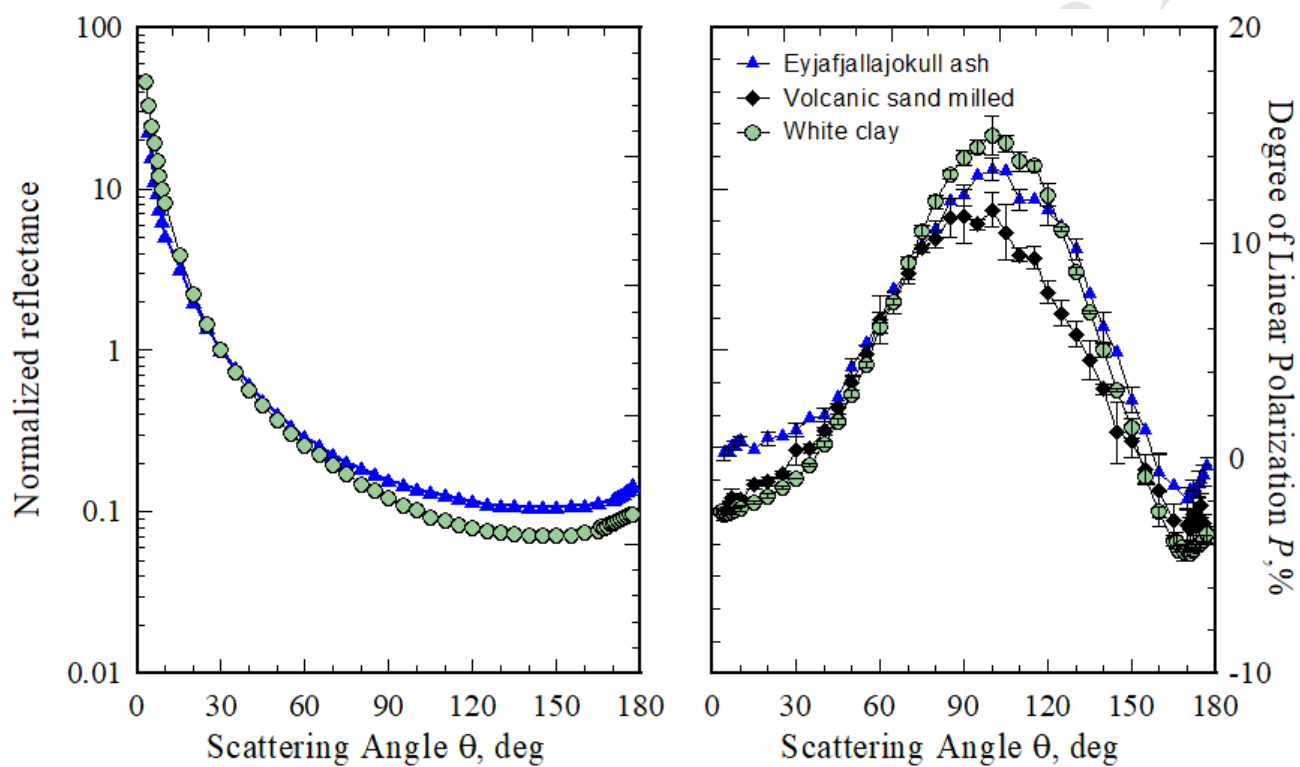
641

642 **Figure 12**

643

644 The normalized reflectance and degree of linear polarization as a function of scattering angle for three
645 different samples: white-clay, milled volcanic-sand, and the ash particles from the Eyjafjallajokull
646 volcano.

647



648

649

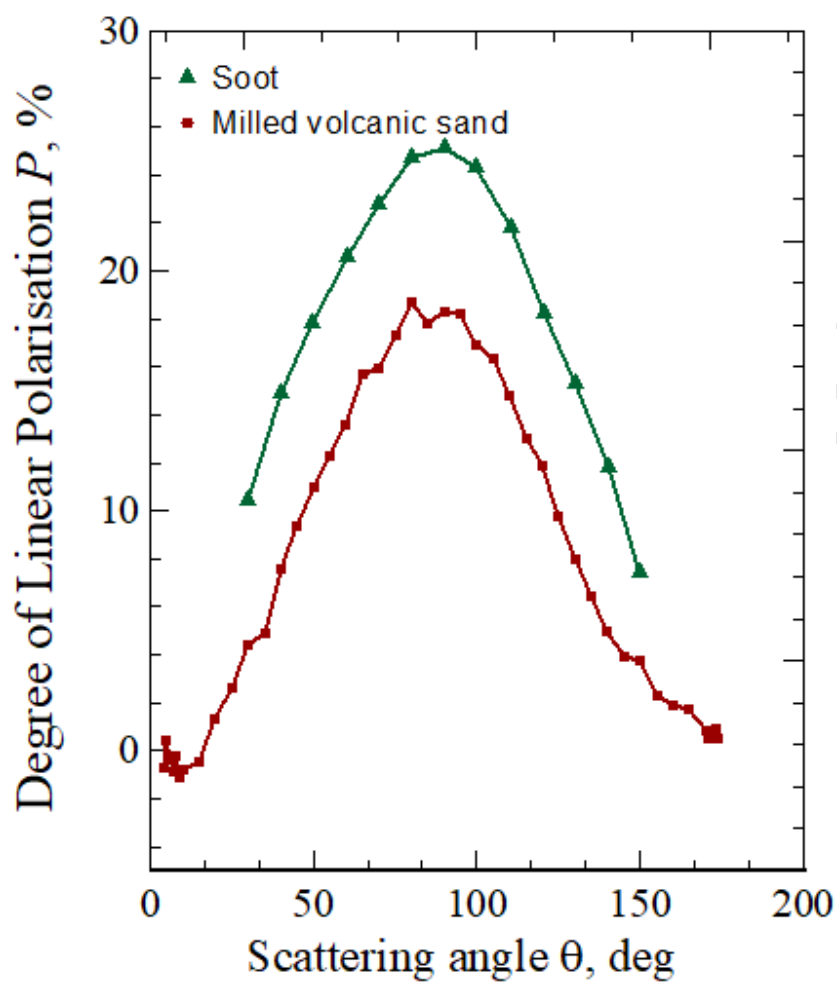
650

651 **Figure 13**

652

653 Comparison of the polarization response of volcanic sand $\lambda = 647$ nm and soot particles at $\lambda = 632.8$
654 nm (data adopted from Francis *et al.* 2011) suspended into the air.

655



656

657 **Figure 14**

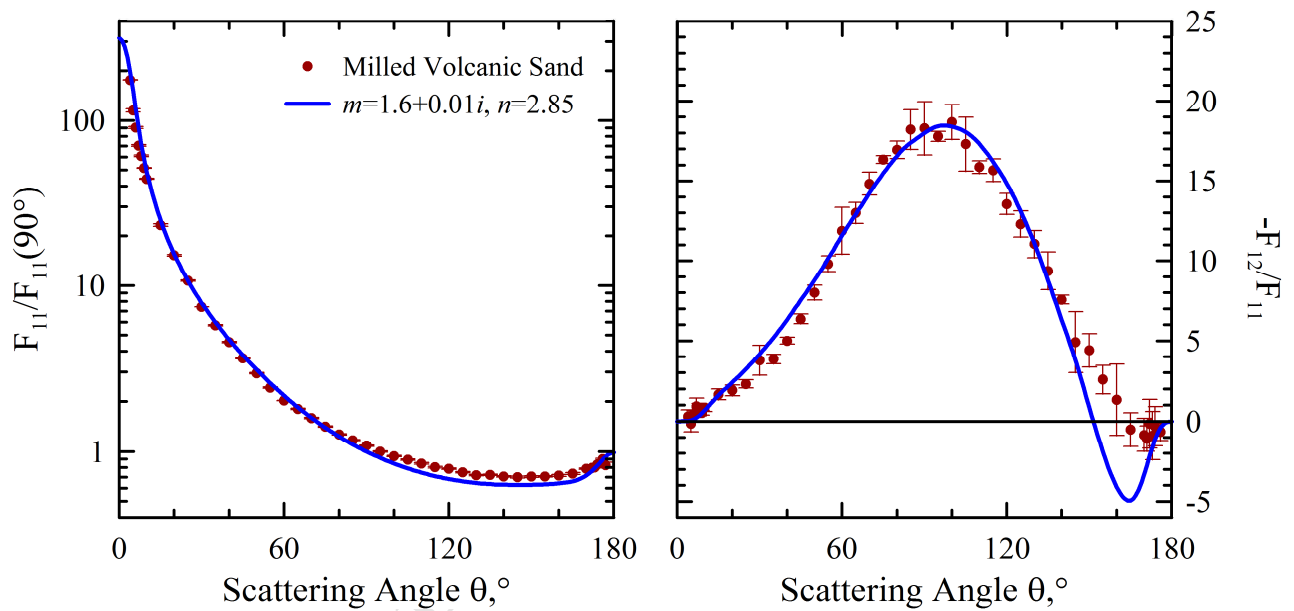
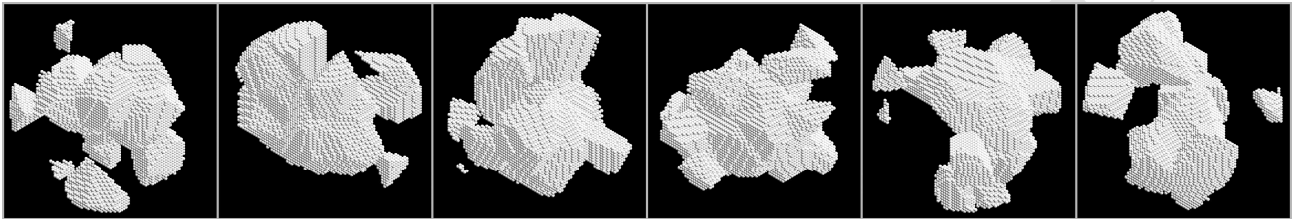
658

659 On the top: Six examples of the modeled agglomerated debris particles. On the bottom: Intensity I (left)

660 and degree of linear polarization P (right) as a function of the scattering angle θ in the milled volcanic

661 sand and their model (blue curve) at $n = 2.85$ and $m = 1.6 + 0.01i$.

662



Research Highlights

- We report angular scattered-light intensity and polarization from the volcanic sand
- Light scattering by volcanic sand is studied in single-particle and deposited modes
- Refractive index of volcanic sand is estimated
- Polarimetric response of volcanic sand is compared to that in carbon-soot